Adaptive Zonal Protection for Ring Microgrids

Uzoma Orji, Christopher Schantz, Steven B. Leeb, James L. Kirtley, Jr., Bart Sievenpiper, Katie Gerhard, and Timothy McCoy, *Senior Member, IEEE*

***Abstract*—In a fault situation on a microgrid with multiple sources, a ring distribution architecture permits healthy parts of the power distribution network to remain operational while isolating a fault. However, fault localization in a multi-ring power distribution system can be considerably more complex than for a radially distributed network. This paper presents a nonintrusive approach for making microgrid protection systems aware of load operating condition in order to improve fault detection, e.g., for detecting destructive high-impedance and arcing faults.**

***Index Terms*—fault protection, microgrids, fault tolerance.**

I. Introduction

FAULT DETECTION on power distribution networks is typically accomplished with protection gear designed to halt operation for current, voltage, or thermal levels in excess of a design threshold. Protection gear has to be sized to permit healthy loads to operate, including permitting adequate margin for in-rush, pulse, or transient electrical demands. Using nonintrusive monitoring, this paper presents an approach for adapting the thresholds of network protection devices based on load operation. High-impedance faults, for example, can occur at current levels below those that would trip fixed-threshold protection gear [1]. This paper demonstrates protection gear with adaptive thresholds that can find subtle faults with greater certainty over a range of load operating conditions.

In a radially distributed network, a source delivers power to a collection of loads organized in a tree structure. Ring distribution, on the other hand, loops the service from a source, through a collection of loads, and back to the source. More than one source may serve the ring. Since the utility can provide power in any direction on the ring, a fault can be isolated, in principle, without interrupting service to many of the loads on the ring [2]. Fault isolation and the ability to flexibly locate sources with respect to loads makes ring architectures attractive for high performance micro-grids designed to remain operating in the face of faults and failures. Multi-ring systems extend this idea, creating a distribution network with several interlocking rings. A variety of power transfer paths may be available, leaving significant flexibility in the event of needed maintenance or a fault on part of the system. However, path multiplicity complicates automatic relaying or protection of a multi-ring system, as it may be difficult to quickly detect and determine the location of a fault and the correct actions to take to minimize customer interruption [1], [3].

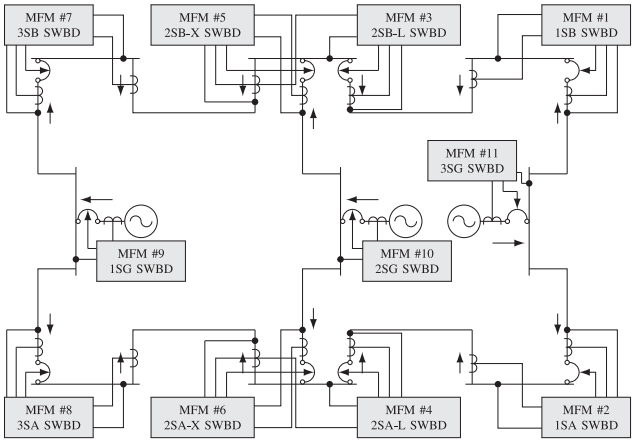

Fig. 1. DDG-51 Flight IIA ZEDS. This diagram includes the addressing, locations and signal inputs of the MFMs. The defined positive direction of current flow is also shown for each MFM (adapted from [11]).

The U.S. Navy has deployed an ingenious system for protecting a multi-ring ac power distribution system on its DDG-51 Arleigh Burke class destroyers. This multiple ring system, or zonal electrical distribution system (ZEDS), is protected by multi-function monitors (MFM) that attempt to isolate faulted sections of the power distribution system while preserving service elsewhere in the ship [5]. A schematic of the alternating current zonal electric distribution system (ACZEDS) found in the DDG-51 Flight IIA destroyer is shown in Fig. 1. The three "straight line" buses in the center of this schematic represent generator switchboards, where the three gas turbine generators on the ship connect to the shipboard power grid. Around the periphery of the schematic, six more buses provide power to radially distributed panel networks (not shown in Fig. 1). The MFM protection units monitor the in-feed and out-feed power to each bus, and have the ability to disconnect one power tie to a bus. The four corner MFM's, numbered 1, 2, 7, and 8, have the ability to completely

Manuscript received August 11, 2015; revised October 25, 2015; accepted December 13, 2015. Date of publication December 31, 2015; date of current version June 19, 2017. Paper no. TSG-00885-2015.

U. Orji and J. L. Kirtley, Jr. are with the Department of Electrical Engineering and Computer Science, Massachusetts Institute of Technology, Cambridge, MA 02139 USA.

C. Schantz is with Tesla Motors, Palo Alto, CA 94304 USA.

S. B. Leeb is with the Massachusetts Institute of Technology, Cambridge, MA 02139 USA (e-mail: sbleeb@mit.edu).

B. Sievenpiper is with the U.S. Navy, Pearl Harbor, HI 96860 USA.

K. Gerhard is with the U.S. Navy, Norfolk, VA 23511 USA.

T. McCoy is with the Electric Ship Office, Washington Navy Yard, Washington, DC 20376 USA.

Color versions of one or more of the figures in this paper are available online at http://ieeexplore.ieee.org.

Digital Object Identifier 10.1109/TSG.2015.2509018

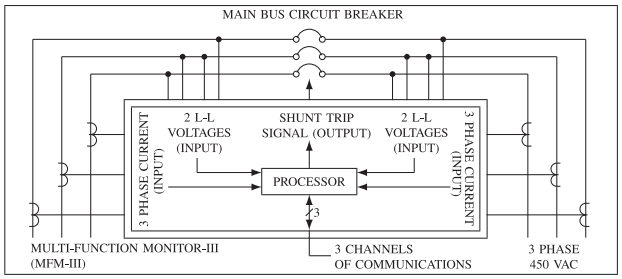

Fig. 2. Functional Diagram of MFM. The diagram shows the sensor layout for the MFM, including three phase current and two voltage measurements per channel. The system includes three ethernet communications channels and a shunt trip output to the associated circuit breaker. (adapted from [11]).

monitor the current flowing to a bus. Considered in pairs, the "center" MFMs, e.g., MFMs numbered 3 and 5, have the information necessary to completely characterize power flow to the middle buses.

With a multi-ring structure like this one, the task of isolating faults becomes more involved than for simpler configurations [12]. More than one decision could be implemented to isolate a fault, and an optimal decision may vary with operating conditions and ship needs. The multi-ring structure protected by MFMs provides a fascinating case study with potential relevance to future microgrids or local utility arrangements that could be "islanded". Comparison of the architecture in Fig. 1 to the grids studied in [1] and [2] show the relevance of the MFM to land-based microgrids, for example. This paper presents techniques for making an MFM-style protection system aware of the operation of "healthy" loads, permitting the MFM to adapt its protection thresholds and detect difficult-to-identify faults like high-impedance faults.

II. Multi-Function Monitor

Figure 2 shows a simplified diagram of the connections to an MFM III. The MFM III controls a contactor or breaker that can open or close an electrical connection to a switchboard. Each MFM III unit measures two line-to-line voltages from two sets of potential transformers and three line currents from two sets of current transformers. The voltage and current sets are separated into left Channel 1 and right Channel 2 signal inputs. Differential signals for current and voltage, or, alternatively, power, can be used to detect faults. The defined positive direction of current flow for each MFM is shown in Fig. 1. Each MFM III unit also has three ethernet ports to send and receive a system information matrix to adjacent MFM III units. Figure 1 illustrates the addressing, locations and signal inputs of the MFMs. The MFM units share information with each other. The MFM III units generate a shunt trip signal when needed to open the associated MFM breaker for fault isolation.

In order for the integrated protective coordination system (IPCS) to work effectively, the MFM III units need to be addressed and numbered so that location-tagged information can be exchanged between the units. By knowing its own address and type, each MFM III can determine its direct neighbors and the remote information necessary to make a shunt trip decision and how to respond during a switchboard fault. Key elements of the IPCS are described below.

A. System Information Matrix

Each MFM III unit learns the status of other units through its dedicated ethernet connections. With status information for all of the MFM units, each unit can make a coordinated response. The system information matrix passed to each unit contains information such as the direction and magnitude of current though each current sensor, circuit breaker status, fault status, switchboard fault status, and shunt trip status.

The fault status of the MFM III unit is determined by the High Speed Relay (HSR) algorithm. Once a fault has been detected and has persisted for sufficient time, the IPCS algorithm seeks to determine the type of fault, i.e., whether the fault is on a switchboard or a bus-tie. Using the information found in the system information matrix, a coordinated response can be made by each unit to send a shunt trip signal to isolate the fault area.

B. High Speed Relay Algorithm

The High Speed Relay (HSR) algorithm uses the current and voltage measurements to assess fault status. Fault detection is a two-step process, beginning with an observed change in voltage magnitude or angle in excess of a tolerance level, followed by a confirmation of an excessive power flow. The details of these routines and outputs are discussed below.

1) HSR Park's Transformation and Fault Trigger: A Park's transformation is used to assess disturbances to system voltage caused by sudden changes in current demand. The MFM uses a fixed sample rate at 2000 Hz, sufficient to resolve current and voltage signals for fault detection without aliasing. Fault detection is based on shifts in magnitude and angle over short windows of utility operation, e.g., eight to ten line cycles, so small errors in the Park's calculation appear not to affect the MFM III in practice. Using the two line-to-line voltage measurements and a balanced three-phase load assumption, the direct (V_d) and quadrature (V_q) components of the voltage are calculated.

The magnitude and angle of the voltage are

$$magnitude = \sqrt{{V_d}^2 + {V_q}^2} \tag{1}$$

$$angle = \arctan\left(\frac{V_q}{V_d}\right). \tag{2}$$

The first stage of the fault detection routine compares the magnitude and angle of the voltage in (1) and in (2) to user-defined thresholds. Magnitude and angle fault flags are set if either of these measurements are outside of specified threshold values, completing the first stage of the fault detection process.

2) Fault Detection and Direction: The algorithm then calculates ΔP, the change in power flow, to confirm and locate the fault. The change in power is calculated as

$$\Delta P = \bar{P}_{fault} - \bar{P}_{SS} \tag{3}$$

where $\bar{P}_{fault}$ is the average fault power and ($\bar{P}_{SS}$) is the average power during normal operation. If the power change is significant, $|\Delta P| \geq \bar{P}_{SS}$, then direction is determined. The fault is

Fig. 3. Examples of switchboard faults.

"downline" if $\bar{P}_{fault}$ is greater than a defined low positive power threshold. The direction is considered "upline" if $\bar{P}_{fault}$ is less than a defined low negative power threshold. The direction is considered undetermined otherwise.

C. Fault Type Determination

The MFM III unit sends a shunt trip signal only if certain conditions are met. The first condition is that the local unit must detect a fault event as specified by the HSR routine. The MFM III unit currently can detect both switchboard faults and bus-tie faults. Each type is discussed below.

1) Switchboard Fault: Figure 3 provides an illustration of a switchboard fault with arrows indicating power directions. If the MFM unit senses fault current flowing into the switchboard from both channels, it makes the determination that there is switchboard fault. The MFM unit can also declare a switchboard fault from over-tolerance conditions on one channel if the MFM is aware of an open breaker that has disconnected the other channel, as shown in Fig. 3. The MFM III is unable to discriminate between a fault at a main switchboard (internal) and a fault below (downstream) of a main switchboard.

2) Bus-Tie Faults: The IPCS algorithm allows the MFM III unit to provide proper isolation of bus-tie faults for both standard and non-standard electric plant configurations. Bus-tie fault detection can be made using both the fault power direction and circuit breaker status or solely on fault current magnitude flags for longitudinal bus-tie faults.

In order to use fault power direction for bus-tie fault detection, local and remote fault power directions must show that power is flowing out of the switchboard from both ends of the bus-tie. For large currents (greater than 6000 A) entering a bus-tie but a small amount of current (less than 600 A) exiting the same bus-tie, then a fault is assumed to exist somewhere on that bus-tie. Cross-tie fault detection cannot use comparisons of the current magnitude flags due to generator contributions to the fault current flowing into the cross-tie.

For longitudinal bus-tie fault events, shunt trip actions will occur if (1) currents on both end are flowing into the bus-tie, or (2) current on one end is flowing into the bus-tie and the other end is open, or (3) the current magnitude flags are set as mentioned before. For cross-tie fault events, IPCS shunt trip action will occur based on either (1) or (2). Figure 4 shows some examples of bus-tie faults.

D. Static Thresholds

The IPCS algorithm makes use of several user-defined thresholds. Initial thresholds used for the HSR routine for fault detection were set based on live tests [13]. The IPCS algorithm

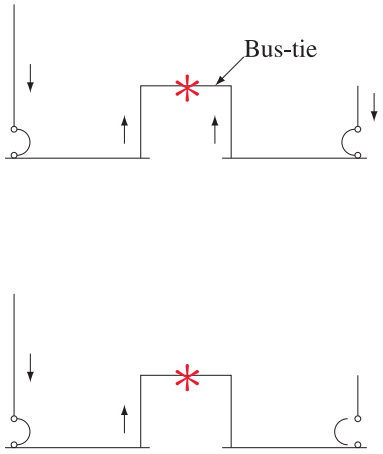

Fig. 4. Examples of bus-tie faults.

also requires that certain time thresholds are met for proper fault identification. The low and high thresholds for voltage magnitude are 0.7 per unit and 1.3 per unit. The maximum allowable angle threshold for the voltage is 15 degrees. The IPCS routine also makes use of duration thresholds to report the various faults. For example, a switchboard fault must exist in the average power for at least 2 ms before an MFM III reports the fault condition. These thresholds are applied to the dynamically evolving average values, so the precise timing of a fault with respect to zero crossings of the voltage waveform will not effect fault detection. Such thresholds were set using DDG-51 Flight IIA computer simulations as described in [11].

Using data exchanged between all of the MFM units, each unit can make a decision about whether or not to open its associated contactor. In the DDG-51 Flight IIA system, the units work, in the presence of a single major fault, to leave half of the ship operational. That is, in a fault situation, one of four reduced operating conditions will occur, leaving active either the three port buses, or the three starboard buses, or the bow or aft rings. Other approaches could also be programmed in principle, e.g., tighter sectioning of the ship to eliminate the very smallest section of the multi-ring network that would remove the fault from the rest of the power system.

Reference [11] states that "future hardware studies may dictate more appropriate delays than those determined through computer simulation." Also, currently, these static thresholds do not adjust based on the state of operation of electrical loads on the ship. Of course, the MFM must be programmed to pass or tolerate the inrush behavior of the largest loads on the power system. These thresholds are fixed, and in particular are not adapted to more conservative levels when the largest inrush loads are already on and operating. We also observe that the MFM III is essentially unaware of harmonic content in the current and voltage waveforms, which could be indicative of fault or abnormal conditions. Most fault protection schemes, for both ac and dc systems, continue to propose fixed design thresholds for determining fault current levels, e.g., [4]. We have been working to demonstrate new approaches for the MFM that permit awareness of operating loads, and that permit adaptive fault thresholds based on load operating state. It is conceivable that an MFM-type device could nonintrusively

track the diagnostic health of critical loads, and also provide a more sophisticated, load-aware protection for the multi-ring power system.

III. Adapting Protection Thresholds in a Ring Bus Power System

If it were possible on a microgrid to know what loads were operating and which loads had yet to be activated, continuously and in real-time, it would be possible to set dynamic protection thresholds. Larger thresholds would be appropriate when larger loads or loads with more substantial transient in-rush currents had yet to be activated. Smaller thresholds with a better chance of detecting subtle faults could be used when it was known with certainty that larger loads had already been activated and reached steady-state operation. In short, fault-detection thresholds could be lowered dynamically and adaptively to catch subtle faults at lower current levels – levels above the needs of yet-to-be activated loads on the network, but below the in-rush demands of operating loads.

Load operating state could of course be determined by submetering every load of interest, at significant expense and complexity. Alternatively, nonintrusive monitoring can detect the activation, operation, and identity of loads on a network in real-time. This information can be used to allow a fault protection system to "know" that loads with significant steady-state or turn-on in-rush current demands are already operating on the network.

A radially distributed power distribution network can be pressed into "dual-use" service, providing not only power distribution but also a diagnostic monitoring capability based on observations of the way in which loads draw power from the distribution service. For the radial segments of a ship's power system, we have developed a nonintrusive power monitor [8], [14], [15] or nonintrusive load monitor (NILM). The NILM detects the activation or operation of loads in near real-time [8]. Algorithms and software for detecting load operation nonintrusively are described in [8] and [9] and are demonstrated in [6] and [7]. Applications of nonintrusive monitoring for condition-based maintenance are described in [10]. This section proposes enhancing protection gear with nonintrusive measurements of load operation.

The nonintrusive approach can be extended to ring networks. With additional signal processing, the DDG-51 MFM protection units, for example, are in nearly perfect locations for performing nonintrusive load monitoring. A new MFM, enabled for nonintrusive power measurements of loads, could become a focal point not only for system protection but also for diagnostics and condition-based maintenance. We also envision that nonintrusive monitoring enhancements could potentially improve the protection function offered by the MFM, by permitting adaptive trip or tolerance setting based on knowledge about active loads on the network.

Zonal electrical distribution systems with a ring architecture have no central monitoring point for load monitoring. Measuring the power draw of monitored loads requires additional computation. In Fig. 1, MFM III units 1, 2, 7 and 8 are "corner" units with complete knowledge of the current flowing into and out of the four "corner" switchboards on the multi-ring system. If I_1 represents the vector of phase currents measured by channel 1 of the corner MFM III units, and I_2 the current vector measured by channel 2, then the vector of switchboard currents I_S can be recovered with Kirchoff's current law (KCL) through computation at the MFM location:

$$I_s = I_1 - I_2. \tag{4}$$

Corner MFM units could easily subtract the currents from both channels to compute I_S, enabling units 1, 2, 7 and 8 to serve as NILM devices monitoring the loads connected to the 1SB, 1SA, 3SB, and 3SA switchboards, respectively.

The middle two switchboards on port and starboard sides of the DDG-51 power system, protected by pairs of MFM-III units 4 and 6, and units 3 and 5, are arranged so that the DDG-51 power system can be reduced in an emergency to half of the system in four quadrants, i.e., a port bus, or a starboard bus, or a forward or aft ring, as appropriate to isolate a fault. This particular arrangement shown in Fig. 1 means that units 3, 4, 5, and 6 cannot individually perform NILM measurements on a switchboard. Whether or not this approach of two MFM's for a switchboard would be desired in other applications, e.g., a land-based islanded grid, would depend on the desired protection scheme. When only "corner" style units are needed to provide protection, the ability to add NILM capability to an MFM-style protection is immediate. When the unit is not a "corner" unit, as in the case for DDG-51 MFM's 3 through 6, NILM capabilities can be recovered by collocating the functions of two of the MFM's in a single unit, i.e., combining the sensor feeds of units 4 and 6 in a single expanded MFM, for example. Or, information could be exchanged between the MFM units, e.g., 4 and 6, over an additional or multi-tasked ethernet link to permit the expanded KCL computation necessary to recover the switchboard current. With any of these approaches, NILM capabilities can be created for any switchboard in the multi-ring distribution system using only existing current and voltage sensors already present for the protection scheme.

Nonintrusive monitoring could enhance MFM operations in at least two ways demonstrated below. First, with awareness of load operation, the MFM could adjust its fault detection thresholds after loads have turned on. For example, there might be no reason to maintain a conservative detection threshold in (3) when known loads with the largest inrush demands on the ring power system have already activated. Fault detection thresholds could therefore be adapted as loads turn on and off. Second, NILM functions could be used to detect unusual harmonic content indicative of pathological conditions. Currently, the MFM makes its decisions strictly based on fundamental frequency power and angle assessment. Certain faults may give tell-tale harmonic signatures that assist with identification.

IV. High-Impedance Faults

The MFM III units currently used in zonal protection employ static thresholds for fault detection. Certain types of faults, e.g., high-impedance faults (HIF), have fault current magnitudes similar to those of normal loads. As a result, normal overcurrent protection devices may not detect and clear

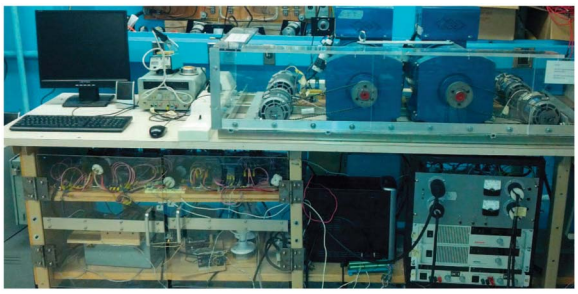

Fig. 5. Scaled hardware model of a shipboard electrical distribution system.

these faults. However, high-impedance faults have waveform characteristics that may serve as telltales [18], [19]. This is a complex subject [20]–[22], and many efforts have been made to characterize the nonlinearity [23], [24], time-varying resistance [25], stochastic, and radio-frequency artifacts of these high-impedance faults [26]–[30].

Faults are inherently not entirely predictable, and we do not seek here to imply that the MFM or any protection system can be made "perfect" for detecting and protecting against all possible faults. Rather, we use two examples to illustrate that, where certain characteristics of a fault or class of faults are known, or where it is desirable to detect and protect in the face of these conditions, the MFM-style ring protection can be augmented to take advantage of this information. Two high-impedance faults examined here are "erratic" high-impedance faults and arcing faults. Figure 2 of [21] illustrates the waveform distortions and randomness exhibited by "erratic" high-impedance faults. An arcing waveform is shown in figure 3a of [25] with distortion due to the non-linear and time-varying grounding resistance. Both types of faults can occur at levels that fail to trip conventional protection gear, but which can still cause substantial damage and fires, especially around combustible materials.

V. Experimental Demonstrations

To demonstrate the potential utility of an MFM unit enhanced with nonintrusive monitoring, a test bench with two 5000 Watt synchronous generators was constructed to emulate a U.S. Navy DDG 51 FLT IIA class ship electric plant as shown in Fig. 5. The standard operating configuration for the DDG-51 zonal electrical distribution system is a maximum of two on-line generators [11]. Therefore, only two generators were used for the test platform even though a DDG 51 FLT IIA class ship is equipped with three generators for redundancy.

A hardware model of a shipboard zonal electrical distribution system was built. More information on the specifications can be found in [31] and [32]. Figure 6 illustrates a one-line diagram of the test stand.

A custom MFM unit was constructed and is equipped with two separate voltage transducer boads to measure two channels of three-phase AC voltage. There are also two sets of current transducers to measure the current in each channel. That is, the MFM test unit reproduces the functionality of the standard MFM illustrated in Fig. 2.

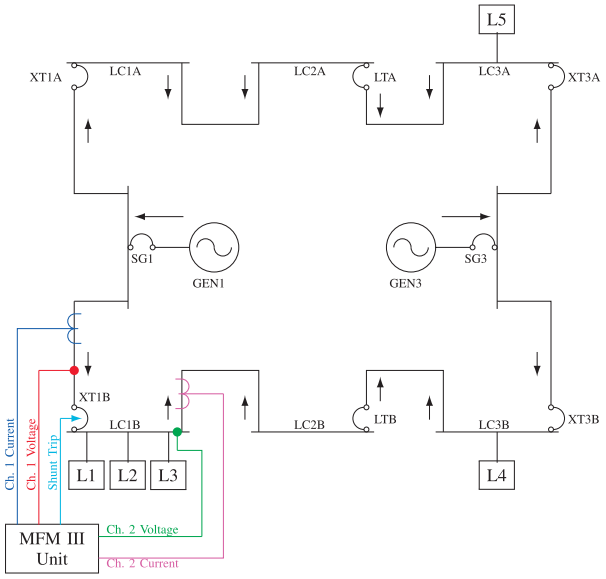

Fig. 6. One-line diagram of ACZEDS hardware model with load configuration.

TABLE I
Loads Used in Laboratory Experiments

Load	Switchboard	Description
L1	LC1B	225 Watt resistive load
L2	LC1B	1/2 HP unloaded motor
L3	LC1B	1 HP loaded motor
L4	LC1A	1/3 HP unloaded motor
L5	LC3A	120 Watt resistive load

To demonstrate the possibilities of a NILM-enhanced MFM III unit, several experiments were conducted with various loads under simulated fault conditions. Table I lists the identifying names, locations, and descriptions of the scale loads used and shown in Fig. 6. The figure also shows the test MFM unit monitoring the LC1B switchboard and the reference directions for power flow.

A. Nonintrusive Disaggregation

By monitoring the currents entering and leaving a given switchboard, a "corner" monitor can use (4) to determine the aggregate current of all the loads connected to the switchboard. To demonstrate this fact, loads L4 and L5 are connected to their assigned switchboards as provided in Table I. Meanwhile, loads L1, L2, and L3 are cycled on and off in succession on the LC1B switchboard.

Figure 7 summarizes results for this experiment. The top plot shows the current in phase A of channel 1 of the MFM unit while the middle plot shows the current in phase A of channel 2. The difference of the two channels is shown in the bottom graph and is the aggregate current drawn by the loads connected to the switchboard.

Load L1 is a resistive load and consumes only real power. Figure 8 plots the total, real, and reactive power draw of the LC1B switchboard during the trial. The first transient response is that of L1 which shows no reactive power draw. The second transient response is for L2, an unloaded

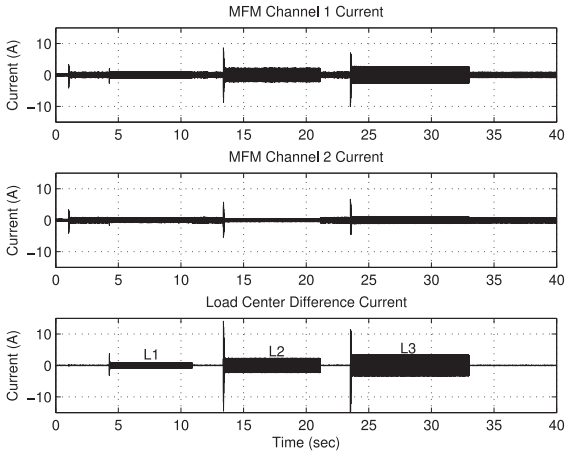

Fig. 7. MFM currents.

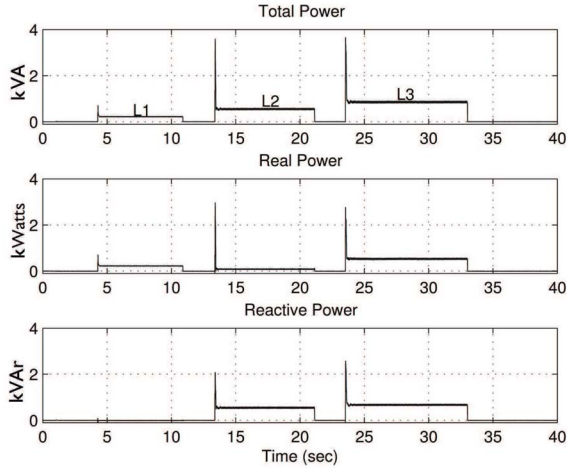

Fig. 8. Total, real and reactive power draw.

induction motor, which draws mostly reactive power. The third transient response comes from L3, a loaded induction motor, which has the largest total power draw from substantial real and reactive power. By analyzing the transient responses and the change in real-power, the NILM-enhanced MFM unit can track loads as they turn on and off.

Figure 9 shows the voltage distortion caused by the turn-on of each of the three loads connected to the LC1B switchboard. Load 3, L3, is the largest real power consumer in the system and exhibits a relatively substantial impact on the voltage waveform measured at the LC1B switchboard when the load is activated. If the load L3 is known to be on, a NILM-enhanced MFM unit could lower the voltage magnitude threshold for fault detection accordingly based on the remaining possible loads in the ship. When L3 is deactivated, the NILM-enabled MFM can automatically increase the fault thresholds to default levels in preparation for a new L3 turn-on transient. In some cases [11], computer simulations can determine the appropriate threshold based on a given set of online loads.

The conventional MFM HSR routine also declares fault conditions based on angle measurements of the voltage. The HSR routine compares the angle with the average of the past eight valid angle samples for angle fault detection. Figure 10 shows

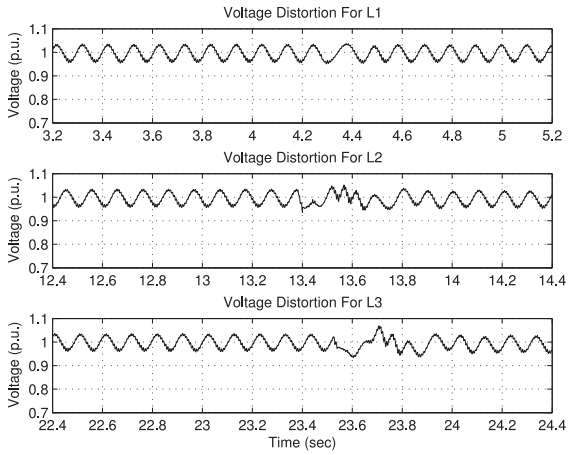

Fig. 9. Voltage distortion for the loads on the LC1B switchboard.

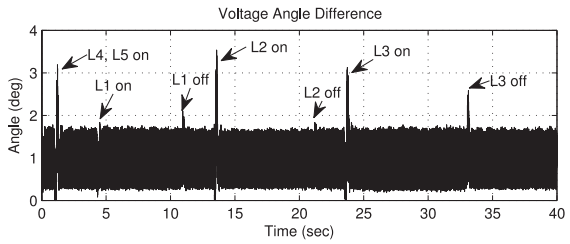

Fig. 10. Angle difference for the loads on the LC1B switchboard.

the angle difference measurements during turn-on transients for L1, L2, and L3. The degree of angle distortion varies with the load. The angle threshold ang_thresh could also be adjusted accordingly as loads come on and off line. The NILM-enabled MFM could also operate with a variable threshold at the second stage of the fault determination process, i.e., a variable threshold for change in consumed power.

B. Switchboard and Bus-Tie Fault Detection

To test capability of our hardware emulator to detect switchboard and bus-tie faults, faults were simulated by switching on sizeable resistive loads on the order of a fault. As described in [13], these were sized to disrupt the bus voltage substantially beyond the fault threshold values.

Loads L4 and L5 remained connected in their respective load centers as specified by Table I. Loads L1, L2, and L3 were turned on in succession. Once all loads were all on, a fault was introduced on the LC1B switchboard. As expected, voltage magnitude and angle measurements are outside threshold values and the faults are detected.

Figure 11 plots the real power in each channel of the MFM unit during the switchboard fault. After time $t = 20.4$ seconds when the fault is simulated, channel 1 on the MFM unit indicates a downstream power flow, while channel 2 indicates an upstream power flow. This combination for a corner MFM unit suggests that power is flowing into the switchboard and consequently a local switchboard fault is detected by the MFM unit.

Figure 12 plots the fundamental real power in each channel of the MFM unit for a fault located on the bus-tie between

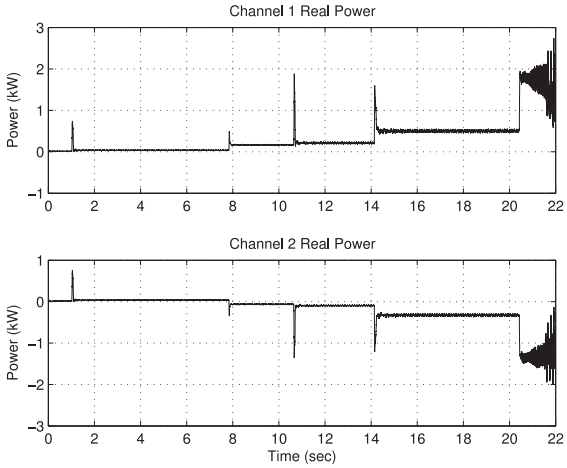

Fig. 11. Real power in both MFM channels during switchboard fault.

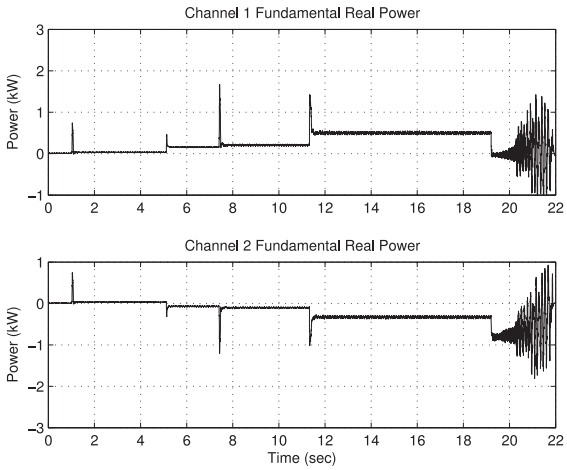

Fig. 12. Fundamental real power in both MFM channels for a bus-tie fault.

Generator 1 and the LC1B switchboard. After time $t = 19.2$ seconds when the fault is simulated, both channel 1 and channel 2 on the MFM unit indicate an upstream power flow. This combination for the MFM unit suggests that the fault is not a local switchboard fault. The fault is either on another switchboard or on a bus-tie.

For these experiments, the simulated faults are sufficiently severe that the voltage magnitude and angle exceed the predefined thresholds and the IPCS routine would begin to isolate the fault area. The experiments discussed below show how high-impedance faults with fault current magnitudes similar to normal loads would not be recognized as faults. New methods for detecting these faults are demonstrated.

C. Detecting High-Impedance Faults

High-impedance faults have fault current magnitudes similar to those of normal loads. Such faults are undetected by the normal overcurrent protection limits and can lead to damaging effects. The high-impedance fault shown in Fig. 2 of [21] was emulated in our hardware test stand with a current controlled load, providing the current waveform shown in Fig. 13.

A variety of load and fault combinations were imposed on the power system to expose an approach for protecting against

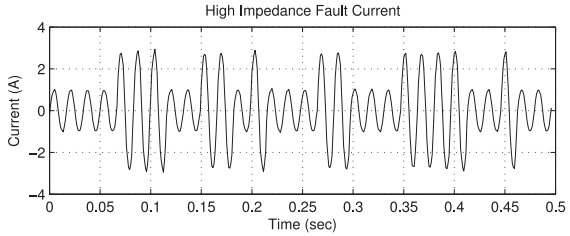

Fig. 13. High-impedance fault current.

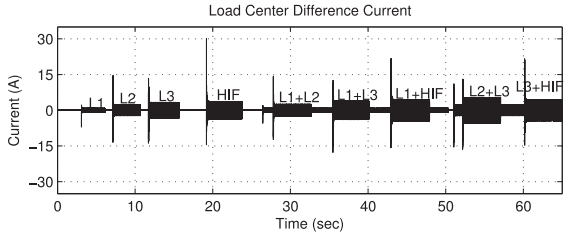

Fig. 14. Current drawn by the loads connected to the LC1B switchboard.

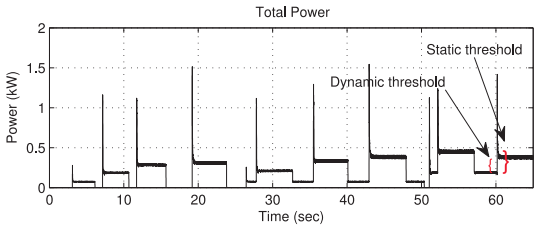

Fig. 15. Total power draw on LC1B switchboard (Load sequence corresponds to Fig. 14).

high-impedance faults in some situations. During this set of experiments, the high-impedance fault was imposed on the LC1B as shown in Fig. 14.

The erratic high-impedance fault current does not exceed the threshold set by the overcurrent protection in the MFM default configuration. In our experiments, the MFM is also capable of nonintrusive monitoring and can extract the LC1B switchboard power using (4). This extracted power is shown in Fig. 15. The fault in this case draws power in excess of the combined loads L1 and L2. With static fault detection thresholds, the MFM protection would be required to pass a "delta" or change in power equivalent to the simultaneous startup of L1, L2, and L3. The HIF in this case would never trip the power change threshold that would cause the MFM to declare a fault. At most, a fault would be declared if most of the loads were operating and the presence of the HIF finally exceeded an absolute maximum current tolerance on the MFM.

On the other hand, as the adaptive monitor recognizes and identifies the activation of particular loads using transient and steady-state power consumption information, the detection thresholds adapt in the monitor to permit just and only the deviations necessary to accommodate the turn-on transients of the remaining loads. The resulting shunt trip signal is shown in Fig. 16. When the power change from the sudden presence of the fault (around 60 seconds into the experiment) exceeds the dynamically variable threshold, the shunt trip is set.

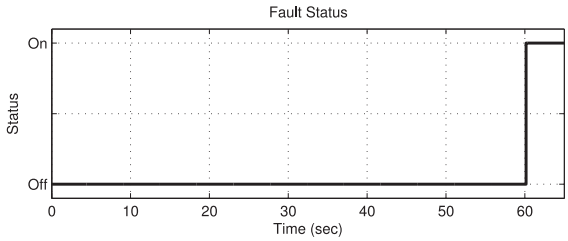

Fig. 16. Shunt trip signal for adaptive MFM.

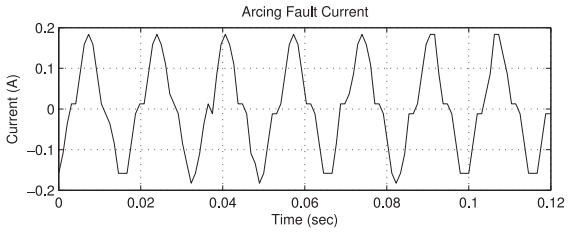

Fig. 17. Arcing fault current.

D. Detecting Arcing Faults

Arcing faults are another type of high-impedance fault that often go undetected for too long. If the fault has harmonic content distinct from the known loads, then harmonic analysis can provide another method for fault detection that is not currently used in the MFM. Figure 17 shows the current waveform of a hardware-emulated arcing fault used in our model power system. This fault is occurs between Phase A and ground. While the ship power system is technically a three wire or delta connected distribution system, the components on the ship are bonded to the hull. The arcing fault examined in this section models a moderate magnitude fault between a phase and a ground-like connection to hull-bonded components.

For this experiment, the "healthy" loads shown in Table I are all balanced three-phase loads. The emulated arcing fault, by contrast, draws significant third harmonic current, and fault detection analysis can be done by monitoring for harmonics. Fault levels or thresholds must of course be set to levels larger than the (dynamically) anticipated third harmonic content created by healthy loads in the grid. Harmonic currents flow in the system impedances, exhibiting harmonic content not only in the aggregate reconstructed current waveform but therefore also inducing third-harmonic voltage distortion. Here, we use voltage harmonic distortion for detecting faults as a demonstration, although harmonic content in either or both current and voltage could be used as a fault detection trigger. The arcing fault load was attached to the LC1B switchboard. With loads L4 and L5 on, loads L2, L3, and the high-impedance arc-fault (HIF) were turned on in a sequence shown in Fig. 18. The top plot in Fig. 19 shows the third harmonic system voltage content. In response to detecting this unexpected harmonic content, the MFM declares a fault condition as shown in the bottom plot of Fig. 19 when the arc fault is present. Note that during transients of loads L2 and L3, there is higher harmonic content flowing in parasitic connections to ground, but the transients do not last long enough to trigger a fault status flag.

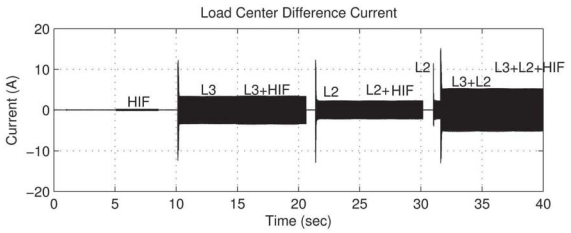

Fig. 18. Current drawn on the LC1B switchboard.

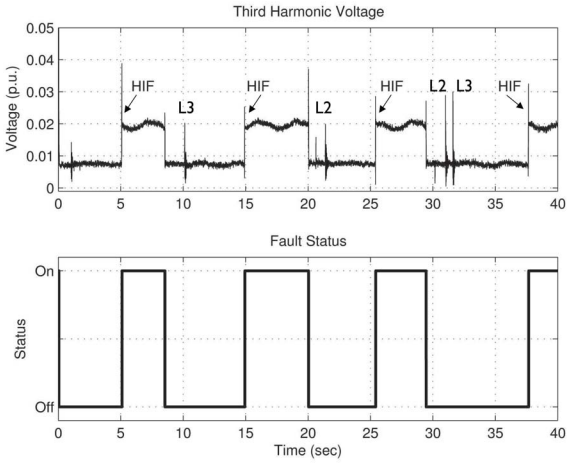

Fig. 19. Third harmonic voltage magnitude and fault status.

VI. Conclusion

Mission critical power systems like those on the DDG-51 have unique concerns and custom protection gear that could guide thinking for the creation of power systems that can be islanded on the land-based utility. The multi-function monitor that protects the DDG-51 multi-ring bus is a rugged and proven protection technology that offers many possibilities for further, intelligent expansion of its protection algorithm. Experiments conducted here demonstrate how the MFM concept could potentially be made adaptive to load behavior for ring or radial microgrids. Such protection gear could defend the power system from subtle faults that fail to create dramatic transients. This protection gear could also serve as a dual-use computation site for energy scorekeeping and for performing diagnostics on critical loads.

References

[1] S. A. Saleh, "Signature-coordinated digital multirelay protection for microgrid systems," *IEEE Trans. Power Electron.*, vol. 29, no. 9, pp. 4614–4623, Sep. 2014.

[2] E. Sortomme, S. S. Venkata, and J. Mitra, "Microgrid protection using communication-assisted digital relays," *IEEE Trans. Power Del.*, vol. 25, no. 4, pp. 2789–2796, Oct. 2010.

[3] M. A. Haj-Ahmed and M. S. Illindala, "Investigation of protection schemes for flexible distribution of energy and storage resources in an industrial microgrid," *IEEE Trans. Ind. Appl.*, vol. 51, no. 3, pp. 2071–2080, May/Jun. 2015.

[4] M. W. Rose and R. M. Cuzner, "Fault isolation and reconfiguration in a three-zone system," in *Proc. IEEE Elect. Ship Technol. Symp. (ESTS)*, Alexandria, VA, USA, Jun. 2015, pp. 409–414.

[5] Naval Sea System Command, "Naval ships' technical manual chapter 320, electric power distribution systems," Nav. Surf. Warfare Center, Carderock Div., Washington, DC, USA, Tech. Rep. S9086-KY-STM-010/CH-320R2, Apr. 1998.

[6] J. Paris, J. S. Donnal, and S. B. Leeb, "NilmDB: The non-intrusive load monitor database," *IEEE Trans. Smart Grid*, vol. 5, no. 5, pp. 2459–2467, Sep. 2014.
[7] M. D. Gillman *et al.*, "Energy accountability using nonintrusive load monitoring," *IEEE Sensors J.*, vol. 14, no. 6, pp. 1923–1931, Jun. 2014.
[8] J. Paris *et al.*, "Scalability of non-intrusive load monitoring for shipboard applications," Amer. Soc. Nav. Eng., Dept. Mech. Eng., National Harbor, MD, USA, Tech. Rep. MITSG 09-23, Apr. 2009.
[9] W. Wichakool, Z. Remscrim, U. A. Orji, and S. B. Leeb, "Smart metering of variable power loads," *IEEE Trans. Smart Grid*, vol. 6, no. 1, pp. 189–198, Jan. 2015.
[10] J. Paris, J. S. Donnal, R. Cox, and S. Leeb, "Hunting cyclic energy wasters," *IEEE Trans. Smart Grid*, vol. 5, no. 6, pp. 2777–2786, Nov. 2014.
[11] Naval Sea System Command, "A guide to MFM III operation," Nav. Surf. Warface Center, Carderock Div., Philadelphia, PA, USA, Tech. Rep. NSWCCD-98-TR-2003/XX, 2003.
[12] L. Plesnick, T. Hannon, and D. Devine, "An intelligent fault detection device for shipboard power systems," in *Proc. Elect. Ship Symp.*, Jun. 2000, pp. 1–6.
[13] D. P. Wipf and B. E. Parker, Jr., "Demonstration and assessment of high speed relay algorithm," Barron Assoc. Inc., Charlottesville, VA, USA, Tech. Rep. N00167-94-C-0083, Jun. 1997.
[14] S. R. Shaw, S. B. Leeb, L. K. Norford, and R. W. Cox, "Nonintrusive load monitoring and diagnostics in power systems," *IEEE Trans. Instrum. Meas.*, vol. 57, no. 7, pp. 1445–1454, Jul. 2008.
[15] J. S. Ramsey *et al.*, "Shipboard applications of non-intrusive load monitoring," in *Proc. ASNE Conf. Survivability Reconfiguration*, Feb. 2005, pp. 1–13.
[16] T. DeNucci *et al.*, "Diagnostic indicators for shipboard systems using non-intrusive load monitoring," in *Proc. IEEE Elect. Ship Technol. Symp.*, Philadelphia, PA, USA, Jul. 2005, pp. 413–420.
[17] W. Greene, J. S. Ramsey, R. Cox, and T. DeNucci, "Non-intrusive monitoring for condition-based maintenance," in *Proc. ASNE Reconfig. Surviv. Symp.*, Feb. 2005, pp. 1–11.
[18] R. D. Christie, H. Zadehgol, and M. M. Habib, "High impedance fault detection in low voltage networks," *IEEE Trans. Power Del.*, vol. 8, no. 4, pp. 1829–1836, Oct. 1993.
[19] M. Aucoin, B. D. Russell, and C. L. Benner, "High impedance fault detection for industrial power systems," in *Proc. IEEE Ind. Appl. Soc. Annu. Meeting Conf. Record*, vol. 2. San Diego, CA, USA, 1989, pp. 1788–1792.
[20] A. A. Girgis, W. Chang, and E. B. Makram, "Analysis of high-impedance fault generated signals using a Kalman filtering approach," *IEEE Trans. Power Del.*, vol. 5, no. 4, pp. 1714–1724, Oct. 1990.
[21] C. L. Benner and B. D. Russell, "Practical high impedance fault detection for distribution feeders," presented at the 40th Annu. Conf. Rural Elect., Fort Worth, TX, USA, 1996, pp. B2–1–B2–6.
[22] S.-J. Huang and C.-T. Hsieh, "High-impedance fault detection utilizing a Morlet wavelet transform approach," *IEEE Trans. Power Del.*, vol. 14, no. 4, pp. 1401–1410, Oct. 1999.
[23] D. Hou and N. Fischer, "Deterministic high-impedance fault detection and phase selection on ungrounded distribution systems," in *Proc. Power Syst. Conf. Adv. Metering Protection Control Commun. Distrib. Res. (PS)*, Edmonton, AB, Canada, 2006, pp. 112–122.
[24] D. Hou, "Detection of high-impedance faults in power distribution systems," in *Proc. Power Syst. Conf. Adv. Metering Protection Control Commun. Distrib. Res. (PSC)*, Clemson, SC, USA, 2007, pp. 85–95.
[25] T. Cui, X. Dong, Z. Bo, A. Klimek, and A. Edwards, "Modeling study for high impedance fault detection in MV distribution system," in *Proc. 43rd Int. Univ. Power Eng. Conf. (UPEC)*, Padua, Italy, 2008, pp. 1–5.
[26] D. Jeerings and J. Linders, "Unique aspects of distribution system harmonics due to high impedance ground faults," *IEEE Trans. Power Del.*, vol. 5, no. 2, pp. 1086–1094, Apr. 1990.
[27] H. Rickover and P. Ross, "Fault protection on shipboard A-C power-distribution systems," *Elect. Eng.*, vol. 63, no. 12, pp. 1099–1120, 1944.
[28] M. Michalik, W. Rebizant, M. Lukowicz, S.-J. Lee, and S.-H. Kang, "High-impedance fault detection in distribution networks with use of wavelet-based algorithm," *IEEE Trans. Power Del.*, vol. 21, no. 4, pp. 1793–1802, Oct. 2006.
[29] C. S. Por, K. L. Choo, and L. Y. Jian, "A study of arc fault current in low voltage switchboard," in *Proc. IEEE Conf. Sustain. Utilization Develop. Eng. Technol. (STUDENT)*, Kuala Lumpur, Malaysia, 2012, pp. 52–56.
[30] S. Liao, R. Zhang, Y. Huang, and H. Xia, "Research of low-voltage arc fault classification based on support vector machine," in *Proc. Int. Conf. Autom. Control Artificial Intell. (ACAI)*, Xiamen, China, 2012, pp. 1690–1693.
[31] C. N. Tidd, "Hardware model of a shipboard zonal electrical distribution system (ZEDS): Alternating current/direct current (AC/DC)," M.S. thesis, Dept. Mech. Eng., Mass. Inst. Technol., Cambridge, MA, USA, Jun. 2010.
[32] J. T. Leghorn, "Modeling for ship power system emulation," M.S. thesis, Dept. Mech. Eng., Mass. Inst. Technol., Cambridge, MA, USA, Jun. 2009.

Uzoma Orji received the Ph.D. degree from the Department of Electrical Engineering and Computer Science, Massachusetts Institute of Technology, in 2013.

Christopher Schantz received the B.S. degree from the California Institute of Technology in 2008, and the M.S. and Ph.D. degrees from the Massachusetts Institute of Technology in 2011 and 2014, respectively, all in mechanical engineering. His research interest lies in signal processing for sensing and control systems. He is currently a Senior Systems Design Architecture Engineer with Tesla Motors (Tesla Motors not affiliated with this research).

Steven B. Leeb received the doctoral degree from the Massachusetts Institute of Technology (MIT) in 1993. He has been a Faculty Member with the Department of Electrical Engineering and Computer Science, MIT, since 1993. He also holds a joint appointment with the Department of Mechanical Engineering, MIT. He is concerned with the development of signal processing algorithms for energy and real-time control applications.

James L. Kirtley, Jr. is a Professor of Electrical Engineering with the Massachusetts Institute of Technology. He was with the Large Steam Turbine Generator Department, General Electric. He was an Electrical Engineer with Satcon Technology Corporation, the Vice President and the General Manager with Tech Center, and a Gastdozent with the Swiss Federal Institute of Technology. He was also a Chief Scientist. He is a specialist in electric machinery and power systems.

Bart Sievenpiper received the Naval Engineer and Master's degrees in mechanical engineering from the Massachusetts Institute of Technology in 2013. He currently serves as an Officer and an Active Duty Engineer in the U.S. Navy.

Katie Gerhard received the Naval Engineer and Master's degrees in engineering and management from the Massachusetts Institute of Technology in 2013. She currently serves as an Officer and an Active Duty Engineer in the U.S. Navy.

Timothy McCoy has served as the Director of the Electric Ship's Office (PMS-320) with the Program Executive Office for Ships, where he was responsible for developing electric power and propulsion systems for the U.S. Navy's fleet. Prior to entering government service, he worked in industry as the Research and Development Director and the President of a defense contractor. He served on active duty in the U.S. Navy. He has published over 35 technical papers. He is a registered Professional Engineer, and a Member of ASNE, IMarEST, and SNAME.